MS5563

Appendix

Probing carbon-bearing species and CO₂ inclusion in amorphous carbon-MgSiO₃ enstatite reaction products at 1.5 GPa: Insights from ¹³C high-resolution solid-state NMR

Kim, Eun Jeong[1]; Fei, Yingwei[2]; Lee, Sung Keun[1,*]

[1]School of Earth and Environmental Sciences
Seoul National University
Seoul, 151-742, Korea

[2]Geophysical Laboratory
Carnegie Institution of Washington
5251 Broad Branch Rd. N.W.
Washington D.C., 20015, USA

[*]Corresponding author,
Lee, Sung Keun
Professor
School of Earth and Environmental Sciences
Seoul National University
E-mail: sungklee@snu.ac.kr
Webpage: http://hosting03.snu.ac.kr/~sungklee
Phone: 82-2-880-6729
Fax: 82-2-871-3269

American Mineralogist

10 pages, 1 Table, and 5 Figures

APPENDIX

A1. Solubility of carbon into crystalline silicates at high pressure up to 25 GPa

The solubility and detailed structure around carbon species in crystalline silicates are often difficult to probe. This is partly because the solubility of the carbon species is relatively low, on the order of 0.01 to 10 ppm (Keppler et al., 2003; Shcheka et al., 2006), and suitable probes are limited. Furthermore, the solubility measurement is often complicated by several extrinsic factors including presence of excess carbon in the grain boundary; the resulting carbon solubility in silicate crystals varied from the order of 0.01 ppm to 2500 ppm (Freund et al., 1980; Keppler et al., 2003; Mathez et al., 1984; Shcheka et al., 2006; Tingle and Aines, 1988; Tsong and Knipping, 1986; Tsong et al., 1985) .

Despite the challenge, previous efforts have provided some insights into carbon species in various silicate crystals at pressures up to 26 GPa (Keppler et al., 2003; Shcheka et al., 2006). The carbon solubility in the silicates does not show a great variation depending on the types and composition of the crystals. The estimated total carbon content in the Mg-silicates apparently increases with increasing pressure, but the formation of Mg-perovskite phase leads to a reduction in the carbon solubility in silicate (Keppler et al., 2003; Shcheka et al., 2006). Table A1 summarizes the estimated carbon solubility in the various silicate polymorphs in a pressure range of 1–26 GPa (Keppler et al., 2003; Shcheka et al., 2006). The solubility of carbon in enstatite at 1.5 GPa varies from 0.05 ppm to 4.7 ppm, which may reside from the carbon contents in the grain boundaries.

Table A1 | Solubility of carbon species in crystalline silicates with varying composition, pressure, and temperature, as reported in previous studies.

Composition	Pressure (GPa)	Temperature (°C)	Duration (h)	Solubility (wt ppm)	Ref.[*]
Enstatite ($MgSiO_3$)	1.5	900–1100	96–168	0.05(1)–0.19(4)	(1)
	1.5	900	96	3.0–4.7	(2)
	6	1100	5	0.38(3)–0.44(3)	(1)
	16	1400	10	0.69(6)–0.80(6)	
Olivine [$(Mg,Fe)_2SiO_4$]	1	1200	34	Not detected	(1)
	1.5	900–1100	144–168	<0.09–0.38(9)	
	1.5	1200	68	0.14(2)–0.25(2)	
	2	1200	71	0.34(4)	
	3.5	1200	71	0.29(4)–0.54(6)	
	7	1200	10	3.27(29)–3.90(68)	
	11	1200	10	11.57(34)–12.75(53)	
Diopside ($CaMgSi_2O_6$)	1.5	900–1100	96–168	<0.01–0.16(2)	(1)
	1.5	900	168	0.4–0.5	(2)
	6	1100	8	1.45(7)–1.60(6)	(1)
Pyrope ($Mg_3Al_2Si_3O_{12}$)	6	1300	10	0.85(5)–0.87(5)	(1)
	6	1300	10	1.9–2.1	(2)
	9	1300	10	0.83(6)–1.27(7)	(1)
	10	1300	6	0.82(4)–0.96(5)	
Spinel ($MgAl_2O_4$)	1.5	1100	168	<0.02	(1)
	1.5	1100	168	Not detected	
Wadsleyite [$(Mg,Fe)_2SiO_4$]	16	1400	10	<0.04–0.04(1)	(1)
	17	1400	4	<0.05	
Ringwoodite [$(Mg,Fe)_2SiO_4$]	21	1200	10	0.04(1)	
	23	1200	4	<0.07–0.10(2)	
Ilmenite ($MgSiO_3$)	25	1400	10	<0.08	(1)
Bridgmanite (Perovskite) ($MgSiO_3$)	25	1400	10	<0.07	(1)
	26	1400	3	<0.05	

[*] (1) Shcheka et al. (2006); (2) Keppler et al. (2003)

A2. The presence of $^{13}CH_4$ in carbon-bearing enstatite by using proton decoupling

Figure A1 shows ^{13}C MAS NMR spectrum for carbon-bearing enstatite with decoupling power of 33 kHz and spinning speed at 11 kHz. Any decrease in the peak width for the peak ~ -9 ppm in Fig. 3 has not been observed. The result may indicate that the small feature at ~ -9 ppm is from background signal.
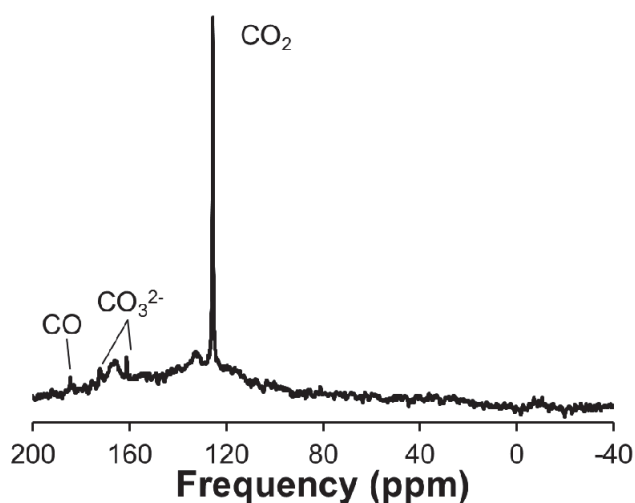

Figure A1| ^{13}C MAS NMR spectrum for carbon-bearing enstatite under proton decoupling with an applied Lorentzian broadening factor of 40.

A3. Effect of residual H in the pressure-induced carbon peak shifts in the amorphous carbon

Protonation into carbon could also affect the observed change in peak position of amorphous carbon under compression. We collected ^{1}H MAS NMR spectra for the compressed and uncompressed amorphous carbon in order to identify whether there would be any ^{1}H reservoir and potential protonation of the sample. The spectra were collected on a Varian NMR system (9.4 T) at a Larmor frequency of 400.01 MHz (3.2 mm double-resonance Varian probe). Single-pulse acquisition with a pulse length of 1.6 μs (radio frequency tip angle of about 30° for solids) was used with a recycle delay of 5 s and spinning speeds of 14 kHz. The potential results would allow us to confirm whether the observed changes in the peak shift is due to residual proton from the H_2O added during the sample synthesis. Figure A2 shows the ^{1}H MAS NMR spectra for ^{13}C-enriched uncompressed and compressed amorphous carbon and those for rotor and stator backgrounds. ^{1}H MAS NMR spectra for rotor and stator background show a broad peak at ~ 7 ppm. The shoulder at ~ -1 ppm is observed for uncompressed amorphous carbon. The assignment of the feature is not trivial, yet previous ^{1}H NMR study for the amorphous carbon under milling showed a broad feature near ~ -1 ppm, assigned to hydrogenated amorphous carbon (Shindo et al., 2011). No noticeable proton peak is observed for compressed amorphous carbon, suggesting the absence of proton reservoir in compressed amorphous carbon. The result confirms that the proton signal from rotor and stator background is far much greater than those from the amorphous carbon and there is no noticeable proton reservoir for the compressed carbon. Taking into consideration negligible H content in the compressed amorphous carbon, it is expected that ^{1}H-^{13}C cross-polarization NMR does not probe the H-C interaction within the amorphous carbon. Indeed, our preliminary ^{1}H-^{13}C cross-polarization NMR spectra for the sample and rotor showed that the most of the signals are from the rotor and stator. The current results again confirm the pressure-induced

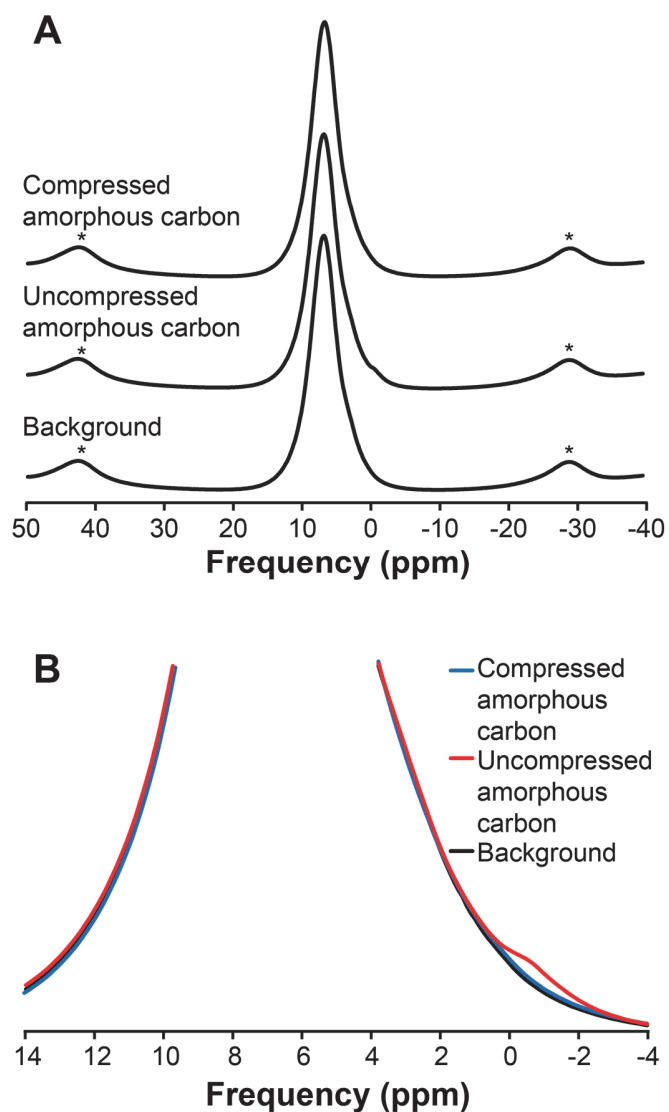peak shift were not affected by the proton in the sample.

Figure A2| (A) ^{1}H MAS NMR spectra for compressed amorphous carbon, amorphous carbon, and rotor-stator background. Asterisks denote spinning sidebands. (B) Expanded ^{1}H MAS NMR spectra for the samples as labeled.

A4. Detection limit on ^{13}C MAS NMR under proton decoupling

Figure A3 shows the ^{13}C MAS NMR spectra for ADM-SiO$_2$ mixtures with varying X_{ADM} ratio with decoupling power of 33 kHz. The spectra show that proton decoupling indeed improves signal-to-noise ratio and ^{13}C MAS NMR spectrum for the sample with $X_{ADM} = 1/259$, ~ 43 ppm can be obtained. See Figure 7 for the calibration results based on the decoupling experiments.
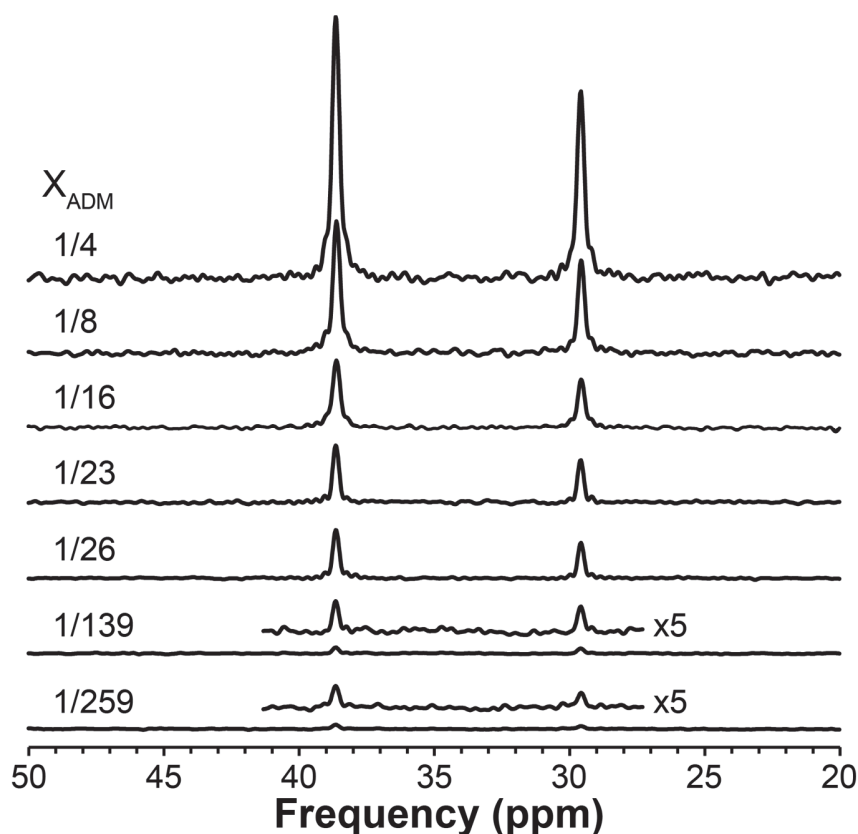

Figure A3| ^{13}C MAS NMR spectra for ADM-SiO$_2$ mixtures with varying X_{ADM} ratio with decoupling power of 33 kHz.

A5. The characteristics of the ^{13}C peak width of various carbonate species

Figure A4 shows the ^{13}C static NMR spectra of 1 M Na$_2$CO$_3$(*aq*) and 1 M (Na$_2$^{13}CO$_3$+NaHCO$_3$)(*aq*), and ^{13}C MAS NMR spectra of calcite and natrite to explore the characteristics of their peak shape in the ^{13}C NMR spectra. The spinning speed for calcite and natrite is 14.7 kHz. The FWHM of calcite and natrite peak in ^{13}C MAS NMR spectra are 0.48 and 0.42 ppm with an employed Lorentzian broadening factor of 10, respectively. The FWHM of 1 M Na$_2$^{13}CO$_3$(*aq*) and 1 M (Na$_2$^{13}CO$_3$+NaHCO$_3$)(*aq*) in ^{13}C MAS NMR spectra are 0.48 and 0.48 ppm with an employed Lorentzian broadening factor of 10, respectively. The FWHM of carbonates peaks in the carbon-bearing enstatite at 161.2, 170.9, and 173.3 ppm are 0.29, 0.37, and 0.35 ppm with a Lorentzian broadening factor of 10, respectively. Therefore, it is difficult to identify their phases (either solid or liquid) based only on their peak widths due to the similarity in FWHM of carbonate minerals and carbonate ions in aqueous solution. Although spectra for aqueous solution collected without spinning at the magic angle, we note that ^{13}C liquid-state NMR under MAS may not reduce the FWHM of the carbonate species in aqueous solution.
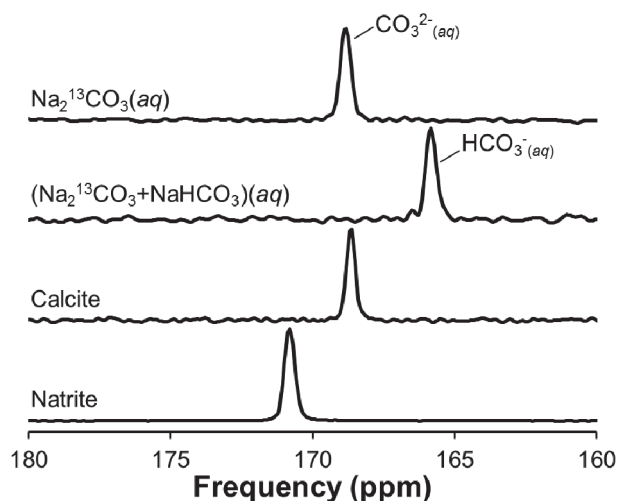

Figure A4| ^{13}C NMR spectra for 1 M Na$_2$^{13}CO$_3$(*aq*), 1 M (Na$_2$^{13}CO$_3$+NaHCO$_3$)(*aq*), calcite, and natrite with an employed Lorentzian broadening factor of 10.

A6. Estimation of the detection limit of carbonate phase in the enstatite-calcite mixture using conventional XRD

In order to test the detectability of carbonate species in the silicate matrix, we collected XRD patterns from enstatite-calcite mixture with varying concentration of carbonate phase (on Rigaku MiniFlex600, using Cu$K\alpha$ X-rays, voltage of 40 kV, current of 15 mA, a 2θ range of 10°– 60°, a step width of 0.01°, and scan rate of 0.4 s/point). Figure A5 shows the XRD patterns of enstatite-calcite mixture with varying $X_{calcite}$ from 0 to 1/32. The calcite (104) peak (red line at 29.4°) intensity can be seen up to $X_{calcite}$=1/256 (~ 0.39 wt%) sample, which is the detection limit with the employed instrument and conditions used in the study. The estimated carbonate concentration is much smaller than the current detection limit of XRD.
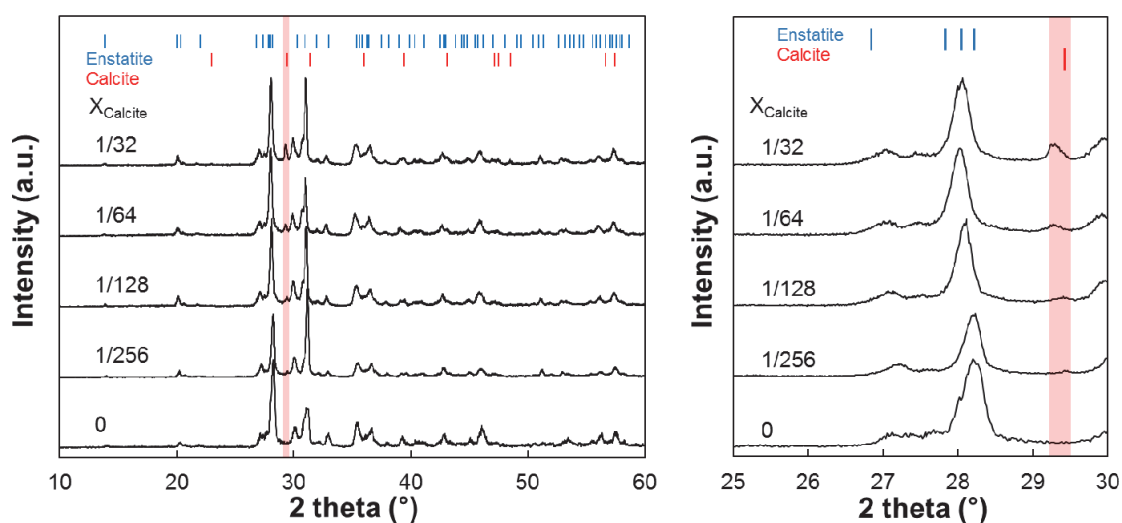

Figure A5| XRD patterns of enstatite-calcite mixture with varying $X_{calcite}$ from 0 to 1/32. Blue and red lines on the top of the figure refer to XRD patterns of enstatite and calcite, respectively. A red area show the decrease of calcite intensity with decreasing $X_{calcite}$ in the sample.

REFERENCES CITED

Freund, F., Kathrein, H., Wengeler, H., Knobel, R., and Reinen, H.J. (1980) Carbon in solid solution in forsterite--a key to the untractable nature of reduced carbon in terrestrial and cosmogenic rocks. Geochimica et Cosmochimica Acta, 44, 1319-1321, 1323-1333

Keppler, H., Wiedenbeck, M., and Shcheka, S.S. (2003) Carbon solubility in olivine and the mode of carbon storage in the Earth's mantle. Nature, 424, 414-416

Mathez, E.A., Dietrich, V.J., and Irving, A.J. (1984) The geochemistry of carbon in mantle peridotites. Geochimica et Cosmochimica Acta, 48, 1849-1859

Shcheka, S.S., Wiedenbeck, M., Frost, D.J., and Keppler, H. (2006) Carbon solubility in mantle minerals. Earth and Planetary Science Letters, 245, 730-742

Shindo, K., Kondo, T., and Sakurai, Y. (2011) ^{1}H NMR study of hydrogen stored in activated carbon powder prepared by mechanical milling. Journal of Alloys and Compounds, 509, 4534-4537

Tingle, T.N., and Aines, R.D. (1988) Beta-track autoradiography and infrared-spectroscopy bearing on the solubility of CO_2 in albite melt at 2 GPa and 1450 °C. Contributions to Mineralogy and Petrology, 100, 222-225

Tsong, I.S.T., and Knipping, U. (1986) Solute carbon and carbon segregation in magnesium-oxide signle-crystals - A secondary ion mass-spectrometry study - comment. Physics and Chemistry of Minerals, 13, 277-279

Tsong, I.S.T., Knipping, U., Loxton, C.M., Magee, C.W., and Arnold, G.W. (1985) Carbon on surfaces of magnesium oxide and olivine single crystals. Diffusion from the bulk or surface contamination? Physics and Chemistry of Minerals, 12, 261-270